IEEE Access
Multidisciplinary ⋮ Rapid Review ⋮ Open Access Journal

Received 8 March 2024, accepted 27 March 2024, date of publication 4 April 2024, date of current version 11 April 2024.

Digital Object Identifier 10.1109/ACCESS.2024.3384868

RESEARCH ARTICLE

Thermal Analysis of Stator Iron-Core-Less PMBLDC Motors Considering Both Winding Eddy and Circulating Current Losses

LIU YANG[1,2,3,4], (Member, IEEE), TIANXIONG GAO[1,3], CHAO AI[1,3], (Member, IEEE), AND XIANGDONG KONG[1]

[1]School of Mechanical Engineering, Yanshan University, Qinhuangdao 066004, China
[2]State Key Laboratory of Fluid Power and Mechatronic Systems, Zhejiang University, Hangzhou 310027, China
[3]State Key Laboratory of Crane Technology, Yanshan University, Qinhuangdao 066004, China
[4]School of Automation, Beijing Institute of Technology, Beijing 100081, China

Corresponding author: Liu Yang (yangliu_ysu@ysu.edu.cn)

This work was supported in part by the National Natural Science Foundation of China under Project 52305073, and in part by the Open Foundation of the State Key Laboratory of Fluid Power and Mechatronic Systems under Grant GZKF-202124.

ABSTRACT Thermal analysis of three stator iron-core-less PMBLDC motors considering winding eddy and circulating current losses is investigated. First, the effects of strand diameter, permanent magnet (PM) magnetization and rotating speed on the above mentioned two winding losses and thermal characteristics are investigated by 3D finite element method (FEM). It is found that both strand diameter and rotating speed have great impacts on the temperature rise, parallel and radial magnetizations have almost identical temperature rise results. Then, influence of eddy and circulating current losses on the thermal characteristics of the three PMBLDC motors are further studied, separately. Furtherly, comprehensive study of the two winding losses on the thermal characteristics is carried out. Results show that thermal analysis considering both winding eddy and circulating current losses in parallel thin strands is vital during motor primary design process considering the limited insulation level of wires and PMs. Finally, three prototypes with different combinations of strand diameters and parallel numbers are selected for the calculation of eddy current losses and temperature rise experiment. Experimental results demonstrate the effectiveness of the developed 3D FEM models and validate the obtained simulation results. This paper clarifies the key influence factors, i.e., windings of different wire diameters, PM magnetization and rotation speed, on temperature rise characteristics of such iron-core-less motors, which provides guidance for the subsequent design of such three types of motors.

INDEX TERMS Stator iron-core-less PMBLDC motor, thermal analysis, winding eddy current loss, winding circulating current loss.

I. INTRODUCTION

High speed iron-core-less permanent magnet (PM) brushless DC (BLDC) motors have been widely used in various applications due to the advantages of high power density, high efficiency, and excellent controllability [1], [2], [3], [4].

The associate editor coordinating the review of this manuscript and approving it for publication was Qinfen Lu.

The weight of the motor can be greatly reduced through the stator iron-core-less design, while the magnetic field distribution in the airgap is much different to that of the stator iron-cored PMBLDC motors [5]. In addition, the phase windings are exposed directly in the high intensity rotating magnetic field because of the non-magnetized epoxy resin substitute the stator iron-core, which will cause additional losses [6], [7]. As the thermal conductivity of the

non-magnetic stator winding frame plastic material is much smaller than that of iron-cored steel, poor heat dissipation and the temperature rise exacerbation of the whole motor will arise. And even the resulted temperature exceeds the conductor's insulation level and cause irreversible PM demagnetization. Thermal analysis, which is closely related to the motor efficiency and operational reliability, plays a vital role in the preliminary design of the motor.

Heat is resulted from losses. For stator iron-cored PMBLDC motors, losses are stator iron loss, copper losses and losses in rotor part [8], [9]. Compared to stator iron-cored PMBLDC motors, the stator iron-core-less PMBLDC motors can eliminate the stator iron loss by using non-magnetized epoxy resin to substitute the stator iron-core of silicon steel, but heavy eddy and circulating currents will be induced in the stator windings. Some studies have been carried out to calculate or reduce the winding eddy and/or circulating current losses, however, papers conducted temperature characteristics only related with the joule loss with ignoration of the winding eddy and circulating current losses. For high rotating speed motors, the pulsations of flux density in the rotor parts, which include the PMs, rotor iron-core and shaft, will cause undesirable rotor losses [10]. The rotor eddy current loss is also related with the space harmonic in the airgap magnetic field, which is related to stator winding forms, PM installation modes [11]. The other influence factor is the armature reaction, which will also cause the magnetic field distortion. And it is mainly related to the control strategy, especially for the PWM driven mode, the rich time harmonics in the winding current will increase eddy current loss significantly.

Many previous studies have identified the main heat sources of electric motor systems as Joule losses and iron losses [12], [13]. Whenever the winding temperature exceeds the maximum values allowed by the insulation class, the insulation life time is heavily reduced by the thermal aging degradation effect [14]. The Joule loss is usually calculated in proportion to the square of the current, which is also known as the dc cooper loss [14], [15], [16], [17], [18]. In [19] and [20], the thermal characteristics of a high-speed PM machine with slotted and slotless stators were evaluated and compared. In [21], the static thermal analysis is discussed in order to validate the proposed cooling system functionality of a coreless PM machine used for flywheel energy storage system. Lee et al. discussed the existence of circulating currents should be considered for safe operation under different levels of manufacturing tolerances for slotless PM motor [19], but the temperature rise caused by the circulating current loss is not mentioned. Accurate and computationally efficient loss prediction is an essential element in thermal analysis of stator iron-core-less BLDC motor, and has become an increasingly important part of the motor design process. Previous papers have done researches on the thermal analysis of traditional BLDC motors, but no literature concentrates on the motors' thermal properties synthetically considering winding eddy and circulating current losses. However, the skin and proximity effects at a high frequency are significant and can greatly increase the ac copper loss. In [22] and [20], finite element method (FEM) is employed to investigate the thermal performance of the stator iron-core PM motors with consideration of the dc and ac cooper loss. In [23], the temperature distribution of a high speed BLDC motor based on the FEM is obtained by accounting for various losses. In [24], the thermal investigation of a surface-mounted PMSM motor is carried out by adopting 3D hybrid analytical modeling, and the accuracy is enabled by considering complex and unsymmetrical actuator housing configurations. Previous studies mostly focused on the temperature rise of iron-cored motors, but researches on the temperature characteristic of stator iron-coreless motors is also pivotal. After study of the loss and temperature rise characteristics, optimization of the motors needs to be carried on. In [25], considering the limitation of thermal characteristics and motor weight, the structure size of motor is optimized by combining finite element analysis with lumped parameter thermal network. In [26], the structure of high loss density and high speed outer rotor surface-mounted permanent magnet motor is optimized by a high computational efficiency thermal research method mentioned in computational fluid dynamics by finite element method. In [27], under the premise of ensuring the output torque, the multi-objective optimization of traction motor is carried out by electromagnetic-thermal 1D simulation method, and the optimal solution of traction motor cross-sectional geometry is obtained. These optimizations are mainly focused on the structure of the motor, and there are few literatures consider the influence of wire diameter and magnetization mode on the temperature rise characteristics of the motor.

In this paper, the thermal characteristics of three stator iron-core-less PMBLDC motors considering both winding eddy and circulating current losses are investigated. Firstly, the specification of the thermal models and heat transfer modes are presented. Secondly, the influence of strand diameter, permanent magnet magnetization and rotating speed on the winding eddy and circulating current losses and the thermal characteristics of the three motors are researched and discussed. Then, the comprehensive effects of circulating and eddy current losses on the thermal characteristic of Type I∼III motors are further studied through 3D FEM. Finally, three combinations of number and diameter of parallel thin strands, i.e., 2 strands @ 0.75 mm, 4 strands @ 0.53 mm, and 11 strands @ 0.31 mm, are selected for the temperature rise experiment to validate the simulated results.

II. ANALYTICAL MODELING AND HEAT TRANSFER

A. MODELING

Fig.1 shows the analytical models of the three stator iron-core-less PMBLDC motor types named Type I ∼ III. Type I motor only contains outer rotor core with PMs mounted on the inner surface and stator windings. Type II motor contains an extra inner rotor core, which rotates synchronously

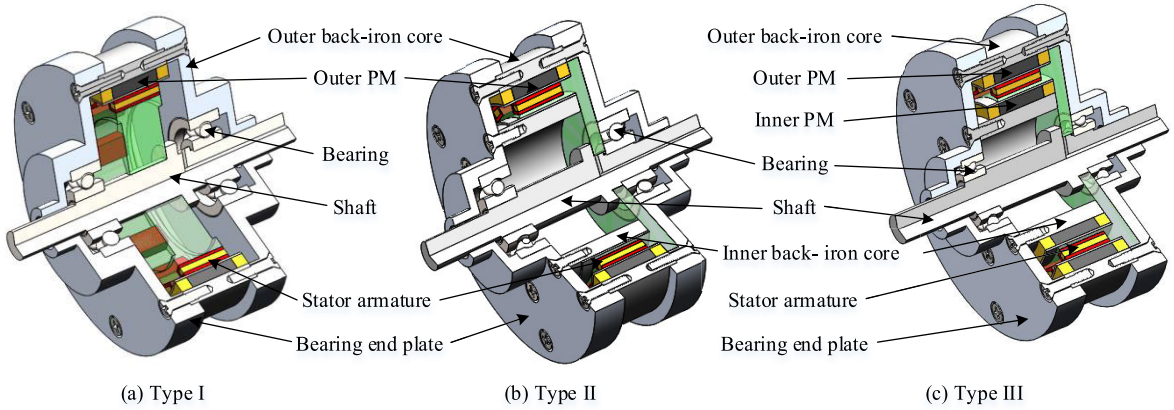

FIGURE 1. Analytical model of the three stator iron-core-less PMBLDC motors. (a) Type I; (b) Type II; (c) Type III.

with the outer rotor core and outer PMs. As for Type III motor, the outer and inner PMs mounted on the corresponding rotor cores, and rotate synchronously with each other. The bearing end plates mount on both ends of the outer rotor iron core symmetrically. And the pole arc to pole pitch ratios of the PMs for the three motors types are 1. Magnetization directions of adjacent PMs in the same sides are inverse with each other and that of the PMs in the same radial direction are the same. 14 poles and 12 slots structures are adopted in the three motor types, such fractional slot machine adopts concentrated winding with each coil around a single tooth to shorten the axial end length of the windings. Nonmagnetic stator core made of epoxy resin material instead of traditional stator iron core is adopted to fix the phase windings. The weight is reduced and the cogging torque is eliminated. However, because of the epoxy resin heat conductivity is much lower than that of iron core, the heat dissipating capability of the motors investigated in this paper is poor. Thus, thermal analysis of the stator iron-core-less PMBLDC motor is vital during the motor primary design.

The specific parameters of the three motors in the paper are given in Table 1.

TABLE 1. Structural parameters of the three motor types.

Symbol	Parameter	Value	Unit
p	Number of pole pairs	7	-
Q_r	Total number of slots	12	-
m	Number of phase	3	-
q	Number of slots per pole per phase	2/7	-
α	Electrical angle of two adjacent slots	210	elec. deg
a	Number of parallel branches per phase	2	-
α_p	Magnet pole-arc to pole-pitch ratio	1	-
U_N	Rated voltage	14	VDC
P_N	Rated power	6	W
I_{phase}	Rated phase current	1	A

B. EDDY AND CIRCULATING CURRENT LOSSES

For the three investigated motors, windings are exposed directly to the high intensity rotating magnetic field, which will cause heavy eddy current loss in the solid conductors. The winding eddy current loss can be obtained through Equ. (1) [28].

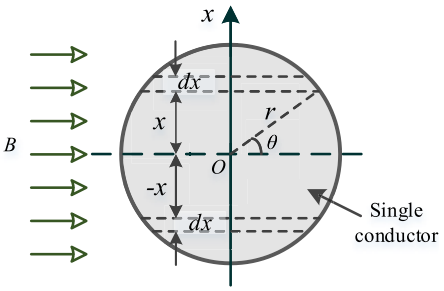

FIGURE 2. Cross section of a single round conductor exposed in magnetic field.

The eddy current loss of the single round conductor can be calculated as

$$\begin{aligned} w_1 &= 16\pi^2 f^2 B^2 \sigma r^4 l \int_0^{\pi/2} \sin^2\theta \cos^2\theta d\theta \\ &= \pi^3 f^2 r^4 B^2 \sigma l \\ &= \frac{1}{16} S D^2 B^2 \omega^2 \sigma l \end{aligned} \tag{1}$$

where r, D, l and S are the radius, diameter, axial length, and cross-sectional area of the conductor, respectively, $\sigma = 5.8 \times 10^7$ S/m is the conductivity of the copper conductor, and $\omega = 2\pi f$ the angular frequency.

Fig. 3 shows the equivalent process of a single conductor wire to multi-strand wire base on same amount of copper. In this way, the eddy current loss can be greatly reduced, however, the circulating current flowing between the thin parallel conductor strand will be increased.

The circulation calculation formula of parallel branch is derived by Kirchhoff law. In view of the fact that the mutual

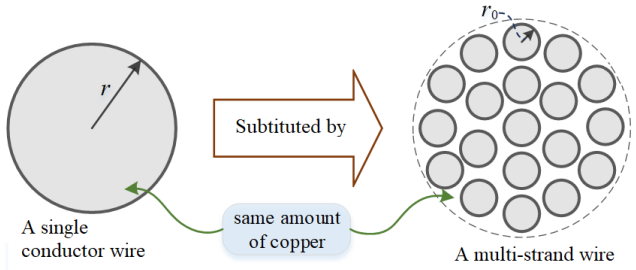

FIGURE 3. Single conductor wire equivalence.

inductance of parallel branches is about one thousand of the self-inductance of each parallel branch, the value is small. Therefore, in the calculation of circulation, the influence of mutual inductance of parallel branches is ignored. According to Kirchhoff voltage law, the strand circulating currents in the phase winding can be calculated by

$$\sum_{k=1}^{\zeta} i_{ck} = \sum_{k=1}^{\zeta} \frac{V - e_k}{\sqrt{(R_k)^2 + (L_k)^2}} = 0 \tag{2}$$

where i_{ck}, e_k, R_k and L_k ($k = 1, 2, 3, \ldots, \zeta$) are the current, induced EMF, resistance and self-inductance of the *k-th* parallel strand, respectively, and V the phase terminal voltage.

The circulating current loss of the whole phase winding, w_c, can be obtained as

$$w_c = \sum_{k=1}^{\zeta} m \cdot a \cdot i_{ck}^2 R_k \tag{3}$$

where a is the number of parallel branches of each phase winding, and m is the number of phases.

C. WINDING EQUIVALENT

Winding equivalent modeling is commonly used in 3D thermal analysis to reduce modeling complexity with acceptable accuracy. The winding equivalent processing is shown in Fig.4. It can be seen from the Eqs. (1)∼(3) that the overall cross-sectional area S of the circular conductor can be guaranteed to be unchanged, and only the effect of conductor wire diameter and rotational speed on the temperature rise characteristics is studied after the equivalent winding, so this equivalent method is reasonable [28], [29], [30].

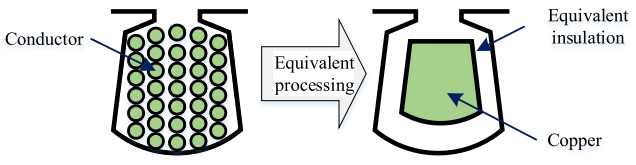

FIGURE 4. Schematic diagram of the winding equivalent processing.

The dosage of winding copper keeps constant during the equivalent process. It can be seen equivalent copper locates at the center of the slot. The region between the equivalent and the slot inner surface is defined as equivalent insulation. It is assumed the equivalent insulation is distributed uniformly around equivalent copper. The material thermal properties of the stator iron-core-less PMBLDC motor components are tabulated in Table 2.

TABLE 2. Material thermal property of the motor different components.

Symbol	Material	Density (kg/m^3)	Specific heat capacity (J/kg·K)	Thermal conductivity (W/m·K)
shell	Aluminim alloy	2700	904	107
shaft	1Cr13	7750	480	50.2
epoxy resin	HT3/5222	1800	1000	0.294
winding	copper	8900	385	400
stator equivalent insulation	-	-	-	0.026
outer rotor iron-core	10#	7900	448	45
copper baffle ring	NdFeB	7500	504	9
bearing	copper	8900	407	387
bearing end plate	9Cr18	7750	480	13.8

The heat conductivity of the equivalent insulation λ_{eq} can be calculated as bellow.

$$\lambda_{eq} = \frac{d_1 + d_2}{\frac{d_1}{\lambda_1} + \frac{d_2}{\lambda_2}} \tag{4}$$

where d_1 is the airgap length; d_2 is the conductor insulation varnish length. λ_1 and λ_2 are the heat conductivities of the airgap and the conductor insulation varnish, respectively.

D. HEAT TRANSFER MODE

As for vacuum and natural environments, the heat transfer modes are somehow different. The thermal radiation in natural environment is as small as to be ignored, while it is a main heat transfer mode in vacuum environment. Due to the operating environment of motor investigated in this paper is natural, heat conduction and convection transfer modes are the two main heat transfer modes. At the same time, considering that the motor structure is enclosed, which make the physical air gap too small to consider. Thus, the air gap between the stator and the rotor can be equivalent to static air and a heat transfer coefficient in thermal modeling [31], [32]. FEM is used to analyze the heat distribution of the stator iron-core-less PMBLDC motor. Fig.5 shows the heat transfer flowing diagram of the stator iron-core-less PMBLDC motor. The arrows mean the heat flows direction. The heat sources in the investigated motors in this paper are the stator winding, PMs, external rotor iron-core and shaft. Along with the heat conduction among different components, and together with

heat convection with the ambient air, the motor reaches to a stable heat transfer condition.

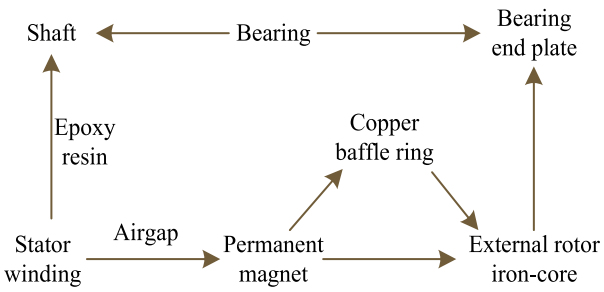

FIGURE 5. Heat transfer flowing diagram of the stator iron-core-less PMBLDC.

Due to the temperature difference between the air medium and motor components, heat convection appears. The first and third boundary conditions are adopted during the thermal simulations. To simplify the calculation, the airgap between the rotor and stator is equivalent to still air with endowed equivalent heat transfer coefficient.

E. POWER CONSUMPTION AND HEAT SOURCE

During the thermal simulation, losses of the heat source are applied to the corresponding components in the form of heating rate. For small stator iron-core-less PMBLDC motors, the heat source mainly comes from the losses of windings and the rotor parts. For the wire gauges used in this paper, the ratio of the resistance between AC to DC for different cases are close to 1. Hence, the proximity and skin effects are neglected in the copper loss calculation here. The losses of phase windings investigated in this paper include the Joule, circulating current and eddy current losses. The Joule loss can be calculated as below.

$$P_{cu} = 3I^2R \tag{5}$$

where I in A is the current effective value of each phase winding; R in Ω is the measured phase resistance.

The winding circulating and eddy current losses are related with the dimension and parallel number of the conductors. It can be found from Fig.1 and Table 1 the materials of both the outer rotor iron-core and the shaft are steel. Hence, heavy eddy current loss will be induced in the high intensity rotating magnetic field.

The heating source rate ζ is calculated based on the volume and the corresponding loss, which can be expressed as (6). Table 3 tabulates the volume of different components of the three motors.

$$\zeta = \frac{W_{loss}}{V_{vol}} \tag{6}$$

where W_{loss} in W is the loss of the heating source; V_{vol} in m^3 is the volume of the component where heating comes from.

The steady-state temperature distribution of the whole model of type I motor at 10,000 rpm is added, as shown in Fig.6. It shows the whole model steady state temperature

TABLE 3. Volumes of different components heating comes form the stator iron-core-less PMBLDC motors.

unit: $\times 10^{-6}$ m^3

	Winding copper	Rotor iron-core	PM	Shaft
Type I	1.12	13.31	6	4.06
Type II	1.12	22.68	6	4.06
Type III	1.12	21.1	10.18	4.45

distribution of Type I motor for the three winding combinations at the rotating speed of 10,000 rpm. Type II and III have the same trend of steady state temperature distribution as type I. It can be found that: 1) the maximum temperatures of Type I motor vary with the three winding combinations are 97.6°C, 197.05°C, 328.91°C, respectively; 2) the highest temperatures appear in the edge of the equivalent winding, because of the heavy winding losses; 3) the second highest temperatures appear in the winding support frame, due to the small thermal conductivity of the non-magnetized epoxy resin.

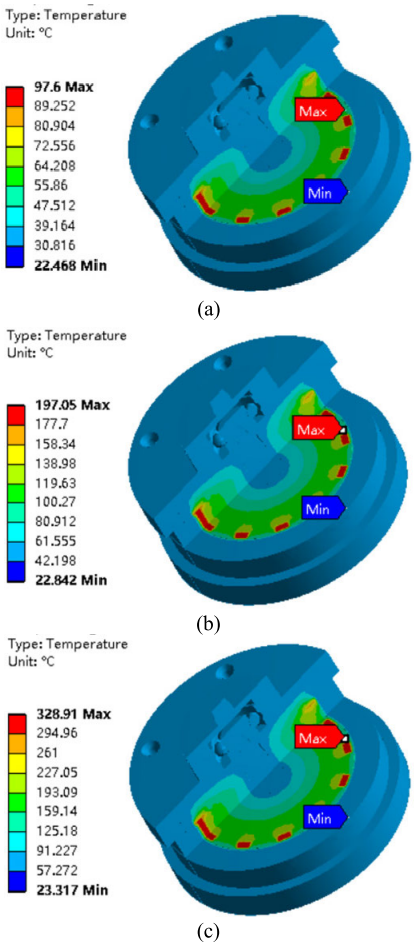

FIGURE 6. Steady state temperature distribution of the stator iron-core-less PMBLDC motor of type I varying with different number and diameter of parallel thin strands at 10,000rpm. (a) 2 strands @ 0.75 mm; (b) 4 strands @ 0.53 mm; (c) 11 strands @ 0.31 mm.

III. FACTORS OF WINDING EDDY AND CIRCULATING CURRENT LOSSES INFLUENCING THERMAL CHARACTERISTICS

The windings are exposed directly in the high intensity rotating magnetic field, and heavy eddy currents are induced in the conductor strands, resulting in the eddy current loss. The larger the diameter of conductors, the higher of the eddy current loss. The larger the diameter of conductors, the higher of the eddy current loss. Then, wires of multi-parallel thin conductors are adopted to substitute the traditional thick conductors to minimize the winding eddy current loss. However, circulating current losses in the parallel thin conductors appears. And the more of the parallel number of the multi-parallel thin conductors, the higher of the circulating current loss. Thus, effects of strand diameter, magnetization types, rotating speed on the temperature rise characteristics and comprehensive effect of the two winding losses are investigated.

A. EFFECT OF STRAND DIAMETER

The winding eddy and circulating current losses with different strand diameters of the three motors with the rotating speed of 10,000 rpm are tabulated in Table 4. It should be stated for Table 4 ∼ Table 6. For each certain diameter of the multiple parallel thin stands, winding eddy current losses increase from Type I to III, and inverse for the winding circulating current losses. Different structures of the three motors induce different air gap magnetic field intensity, Type III motor maintains the highest magnetic flux density, and type I motor possesses the smallest. Moreover, Type III motor obtains the most uniform magnetic field distribution due to its dual rotor structure, which results in the smallest circulating current loss. For the three motors, the eddy current losses increase with the enlargement of wire diameter, and the circulating current losses gradually decrease as the wire diameter increase (the number of parallel windings gradually decreases). The above discussion indicates the importance of the choice of wire diameters on overall consideration of the winding eddy and circulating current losses of stator iron-core-less PMBLDC motors.

The steady state temperature rise along with the linear increasement of the multiple parallel thin strands diameters of the three motors are illustrated in Fig.7.

TABLE 4. Winding eddy and circulating current losses versus strand diameters with rotating speed of 10,000 rpm.

unit: W

Type		Strand diameter (mm)						
		0.3	0.5	0.7	0.9	1.1	1.3	1.5
w_e	I	3.5	5.02	7.2	10.33	14.81	21.23	30.44
	II	4.71	6.5	8.98	12.39	17.1	23.61	32.58
	III	8.47	11.4	15.34	20.66	27.81	37.44	50.4
w_c	I	35.78	20.67	7.6	4.04	3.72	3.53	3.41
	II	20.28	11.9	4.9	3.28	3.21	3.16	3.14
	III	5.73	4	2.8	2.6	2.6	2.59	2.59

w_e: eddy current loss; w_c: circulating current loss

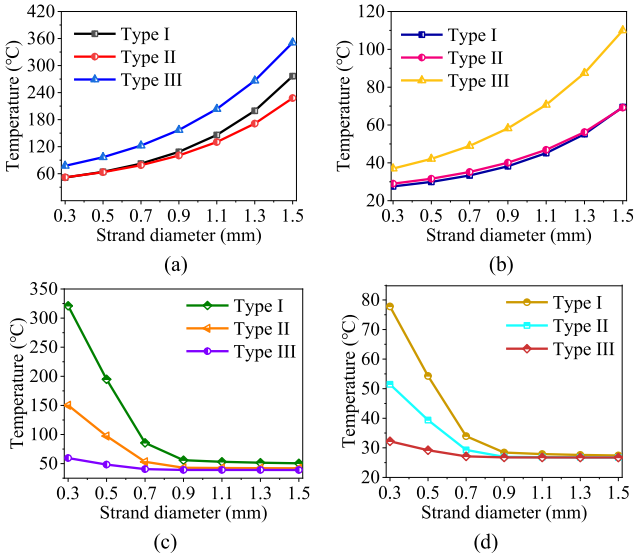

FIGURE 7. Steady state temperature rise of the three motors varying with different diameters of the multiple parallel conductor strands with the rotating speed of 10,000 rpm under parallel magnetization. (a) winding temperature with winding eddy current losses; (b) PM temperature with winding eddy current losses; (c) winding temperature with winding circulating current losses; (d) PM temperature with winding circulating current losses.

For each type motor, the steady state temperature with winding eddy and circulating current losses for both winding and PM increase nonlinearly along with the linear increasement of the parallel thin strands' diameter. And the steady state temperature rise with winding eddy current loss of windings and PM for Type III motor keeps the largest, and that with winding circulating current loss keeps the smallest, which fits the losses variation in Table 4. Specially, for Type III motor, when the strand diameter above 1.1 mm, the winding temperature induced by eddy current reaches 180 °, which exceeds the maximum temperature resistance level of the winding insulation. As for Type I motor, when the strand diameter less than 0.5 mm, the winding temperature caused by the circulating current rises over 180 °C. Thus, it can be concluded strand diameter has great influence on the temperature characteristics of the three motors, especially on the winding part.

B. EFFECT OF MAGNETIZATION

The winding eddy and circulating current losses of the three stator iron-core-less PMBLDC motors with strand diameter of 0.3 mm and two different magnetizations are calculated and tabulated in Table 5, and the rotating speed is set to 10,000 rpm. It can be found that both the winding eddy and circulating current losses with radial magnetization just a little higher than that of the parallel magnetization.

Fig.8 plots the winding and PM steady state temperature rise of the three motors with parallel and radial magnetizations. The temperature rise of the two different magnetizations show little difference for three motors. The winding and PM temperature rise of radial magnetization

are 2.7% and 1% higher than that of the parallel magnetization, respectively, for the case of winding eddy current losses. For the case of winding circulating current losses, the winding and PM temperature of radial magnetization increase by 4.6% and 1.2% than that of parallel magnetization, respectively.

Under each type of magnetizations, the winding and PM temperature with eddy current losses of Type I motor maintain the smallest than the other two type motors. But when considering the circulating current losses, the results become completely opposite, the winding temperature of Type I is as high as 320 °, which is much higher than the maximum temperature resistance level of winding insulation. It can be obtained the PM magnetizing types have little influence on the temperature rise characteristics for the three investigated motors. However, due to the structural difference, the steady state temperature characteristics for different type motors is somehow different. Therefore, it is necessary to consider the impact of the circulating current on the motor temperature rise characteristics.

TABLE 5. Winding eddy and circulating current losses with two different magnetizations of the three motor types.

unit: W

Type	Radial magnetization		Parallel magnetization	
	w_e	w_c	w_e	w_c
Type I	3.76	36.69	3.5	35.78
Type II	4.99	22	4.71	20.28
Type III	8.55	6.13	8.47	5.73

w_e: eddy current loss; w_c: circulating current loss

C. EFFECT OF ROTATING SPEED

For the three motors with strand diameter of 0.3 mm, the winding eddy and circulating current losses versus the rotating speed are tabulated in Table 6. As shown in Fig.7 and Fig.9, the steady state temperature rise law with rotating speed is similar with strand diameter. For each type motor, the winding eddy and circulating current losses increase with the rotating speed. For a certain rotating speed, the winding eddy current losses increase from Type I to III, and the winding circulating current losses decrease from Type I to III.

The variation of steady state temperature rise of winding and PM with rotating speed of the three type motors are shown in Fig. 9. It can be observed the winding and PM temperature of the three motors increase with the rotating speed, which is the same trend as the losses tabulated in Table 6. In terms of winding eddy current losses, the winding and PM steady state temperature of Type I keep the smallest along with the rotating speed variation, and the winding temperature of Types I and II almost equal to each other during the speed ranging from 6,000 rpm to 10,000 rpm. The winding temperature rise rate of Type III

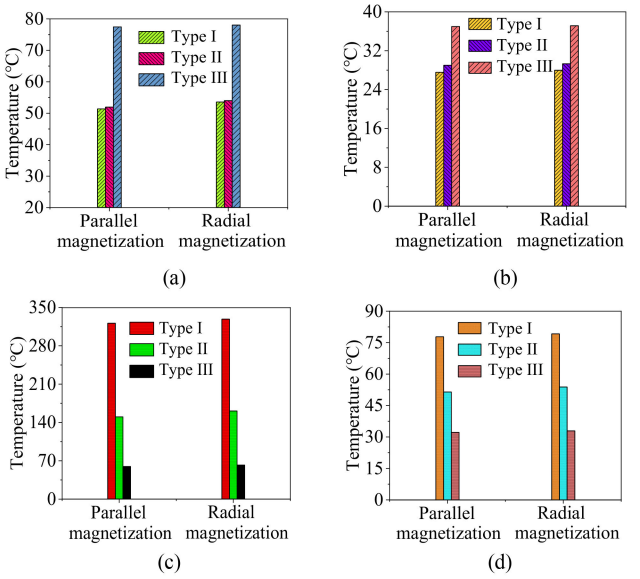

FIGURE 8. Steady state temperature rise of the three motor types varying with two different magnetizations with strand diameter of 0.3 mm and rotating speed of 10,000 rpm. (a) winding temperature with winding eddy current losses; (b) PM temperature with winding eddy current losses; (c) winding temperature with winding circulating current losses; (d) PM. temperature with winding circulating current losses.

become much bigger than that of Type I and Type II. On the contrary, the winding and PM temperature with circulating current losses of each type motor show the reverse effect. Especially when the rotating speed over 8,000 rpm, the winding temperature rise of Type I motor exceeds the maximum temperature resistance level of 180 °C. The winding temperature rise of Type II motor exceeds 180 °C when the rotating speed over 11,000 rpm. Moreover, when the type I motor rotates at 15,000 rpm, the PM temperature reaches approximately 140 °C, which is close to the maximum operating temperature of NdFeB (150 °C), affecting the working performance of the permanent magnet and may cause PM irreversible demagnetization. It can be concluded that, for the three stator iron-core-less PMBLDC motors, especially in high-speed operation, it is necessary to consider the influence of circulating current on the temperature rise characteristics.

TABLE 6. Winding eddy and circulating current losses versus rotating speed of the motors with strand diameter of 0.3 mm.

unit: W

Type		Strand diameter (mm)				
		6000	9000	10,000	12,000	15,000
w_e	I	2.91	3.32	3.5	3.9	4.64
	II	3.42	4.46	4.71	5.92	7.8
	III	4.73	7.42	8.47	11.17	16.01
w_c	I	14.48	29.48	35.78	50.28	77.18
	II	9.51	18.21	20.28	30.37	45.99
	III	3.73	5.17	5.73	7.18	9.77

w_e: eddy current loss; w_c: circulating current loss

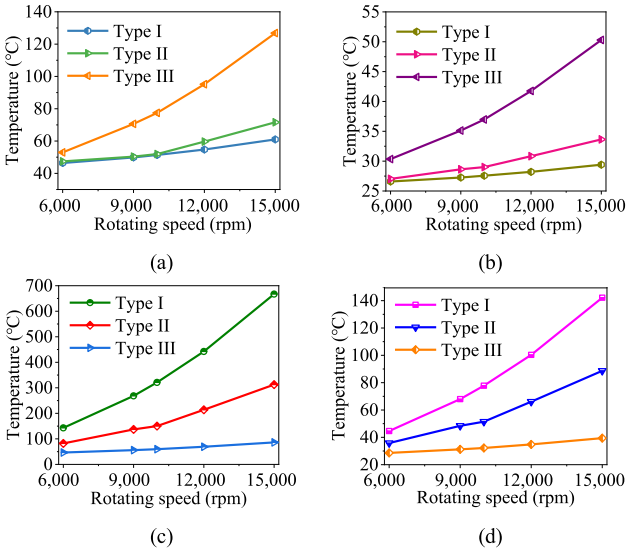

FIGURE 9. Steady state temperature rise of the three motors versus rotating speeds with strand diameter of 0.3 mm and parallel magnetization. (a) winding temperature with winding eddy current losses; (b) PM temperature with winding eddy current losses; (c) winding temperature with winding circulating current losses; (d) PM temperature with winding circulating current losses.

D. COMPREHENSIVE EFFECT OF CIRCULATING AND EDDY CURRENT LOSSES

Due to the structural difference of the three type motors, the winding circulating current losses with a certain strand diameter decrease from Type I to Type III. However, the eddy current losses are converse. Hence, the sums of the winding eddy and circulating current losses for the three motors investigated in this paper are different with each other, which results in different temperature rise characteristics. Three combinations of number and diameter of parallel thin strands, i.e., 2 strands @ 0.75 mm, 4 strands @ 0.53 mm, and 11 strands @ 0.31 mm of three motors are selected for the thermal analysis, which are synthetical accounting for the winding eddy and circulating current losses. The winding losses, including Joule losses and the circulating and eddy current losses versus rotating speed are tabulated in Table 7.

Fig.10∼Fig.12 show the temperature variation versus the rotating speed for the three winding combinations mentioned above. For three different combinations of number and diameter of parallel thin strands, similarities and differences coexist in the trends of winding and PM temperature rise versus the speed of the three motors. In terms of similarities, the temperatures of both winding and PM increase gradually and nonlinearly with the rotating speed. The winding temperature are 2.1∼4.7, 1.9∼3.6, 1.9∼3.0 times higher than that of PMs with the rotating speed ranging from 6,000 rpm∼15,000 rpm for the three motors. For a certain rotating speed, with the increase of parallel strand number and decrease of strand diameter, the winding and PM temperature rises of Type I and Type II motors increase gradually, but decrease for that of Type III motor. Specifically, when the rotating speed changes from 6,000 rpm ∼15,000 rpm, winding temperature rises of 11 strands @ 0.31 mm case are 2.3∼4.2 times than that of 2 stands @ 0.75 mm case, and 1.6∼2.4 and 0.9∼0.7 for Type II motor and Type III motor, respectively.

TABLE 7. Winding eddy and circulating current losses versus rotating speed of the three motors with three motors with three combinations of number and diameter of parallel thin strands.

unit: W

Type		Rotating speed (rpm)				
		6,000	9,000	10,000	12,000	15,000
2 strands @ 0.75 mm	I	4.9	7.79	9.02	11.84	17.04
	II	5.28	8.69	9.5	13.43	19.53
	III	7.39	13.4	15.73	21.79	32.61
4 strands @ 0.53 mm	I	9.18	17.35	20.92	28.89	43.76
	II	7.27	13.16	14.57	21.39	31.97
	III	6.36	11.07	12.9	17.65	26.14
11 strands @ 0.31 mm	I	14.81	30.22	36.7	51.6	79.24
	II	10.34	20.08	22.41	33.7	51.2
	III	5.88	10.01	11.61	15.77	23.2

Combined with the research results of the effect on strand diameter in Section II, the influence of circulating current loss on winding and PM temperature rises of Type III motor is not obvious due to its uniform magnetic field distribution caused by dual-rotor structure. The temperature rise of Type I and Type II motors are influenced by the winding eddy and circulating current losses. Therefore, thermal analysis synthetically accounting for the eddy and circulating current losses in parallel thin strands is vital during the primary motor design process. For instance, the temperature of winding for 4 strands @ 0.53 mm is over 180 °C at 10,000 rpm, which exceeds its insulation level of Type I motor.

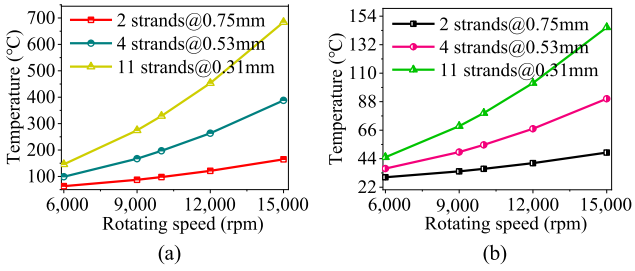

FIGURE 10. Steady state temperature rise of Type I motor with three different winding combinations versus rotating speed. (a) winding; (b) PM.

IV. EXPERIMENTAL TESTING

A. EXPERIMENT FOR WINDING EDDY CURRENT LOSS

The winding bracket and combinations of number and diameter of strands under the Type I motor structure are shown in Fig.13. The three wire diameter combinations are 2 strands @ 0.75 mm, 4 strands @ 0.53 mm, and 11 strands @ 0.31 mm. The PMs of the three prototypes of Type I motor are with parallel magnetization.

Fig.14 shows the winding eddy current loss test platform. The winding eddy current loss of the motor can be measured

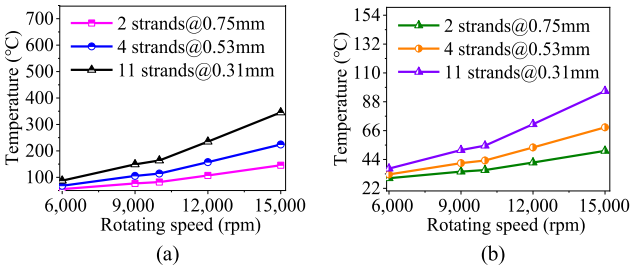

FIGURE 11. Steady state temperature rise of Type II motor with three different winding combinations versus rotating speed. (a) winding; (b) PM.

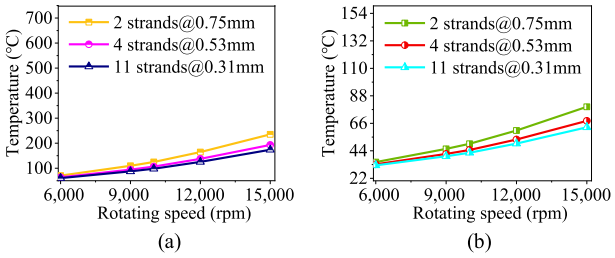

FIGURE 12. Steady state temperature rise of Type III motor with three different winding combinations versus rotating speed. (a) winding; (b) PM.

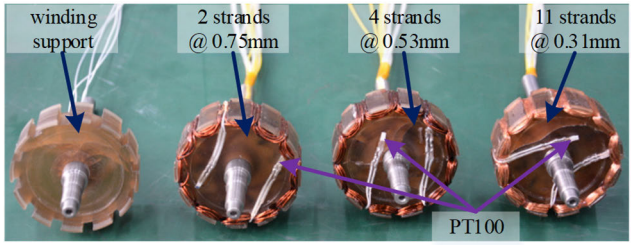

FIGURE 13. Stator prototypes of Type I motor of three combinations of number and diameter of strands for experimental testing.

for the three cases by the free stopping and loss separation methods. Towing motor speed is 3000 rpm, used to drive the test motor. Assuming J (kg·m^2) is the inertia of rotating parts of the driving motor, torque sensor, coupling and the test motor. The angular acceleration versus time can be obtained by the derivation of the free speed dropping curve, which is collected from torque sensor. The eddy current loss of the test motor system, w, can be calculated by Eq. (7) as below. And the total loss is the integral of w in the whole free stopping time. One can express the winding eddy current loss, as the difference between the losses of stator support with and without phase windings.

$$\begin{cases} T = J \cdot \beta \\ w = T \cdot \omega \end{cases} \tag{7}$$

where T is the torque in Nm produced by the loss, β the angular acceleration in rad/s^2, and ω the angular velocity in rad/s.

Figure 15 shows the simulation results and experimental results of eddy current loss of Type I motor winding under

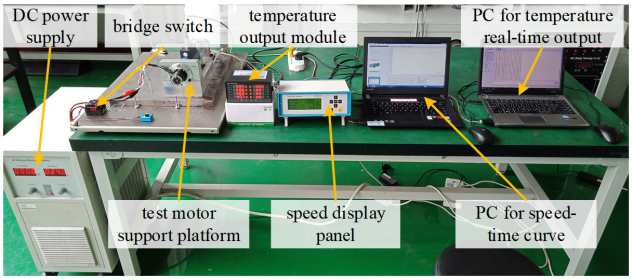

FIGURE 14. Winding eddy current loss test system.

three wire diameter combinations. It can be seen that the winding eddy current loss of the thin strands motor is lower than that of the thick strands motor, which agrees with the previous analysis. The experimental results have also shown good agreement with the FEA results. The small difference between the FEA and experimental results in the case of 2 strands @ 0.75 mm can be attributed mainly to the difference of bearing pre-tightening before and after the change of stators.

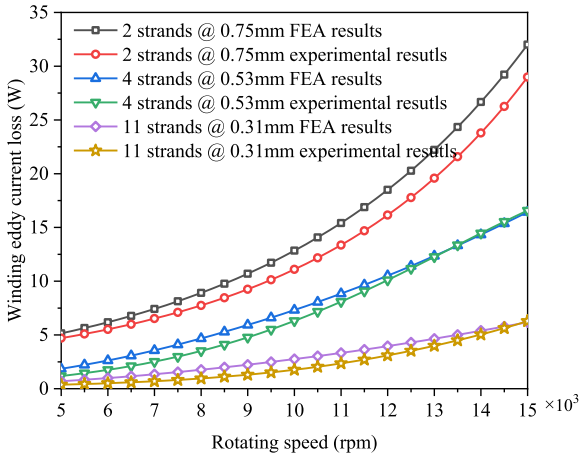

FIGURE 15. The 2D FEA and experimental test results of winding eddy current losses of Type I motors with three combinations of number and diameter of strands versus rotating speed.

B. EXPERIMENT OF MEASURING TEMPERATURE RISE

In order to calculate the temperature rise at different positions of the stator winding, five measured positions (P1∼P5) are selected, which includes the slot side edge, the center of the windings in the individual slot, the bottom of the individual slot, the end of the windings, the end of the winding support, respectively. Temperature rise of five stator positions are measured through the embedded temperature sensors for every prototype stator.

Fig.13 shows the nonmagnetic winding supports installed with the above mentioned three combinations of number and diameter of parallel thin strands. Besides, two temperature sensors were installed in the slot and on the end of the winding support, as it shows in the left side of Fig.13. It is used to

eliminate the temperature error caused by the bearings and the windage friction loss.

Fig.16 shows the temperature rise test system of the outer rotor and stator iron-core-less PMBLDC motor of Type I. The test motor is driven by a high-speed BLDC motor with the rated speed of 30,000 rpm. The temperatures of the five measured positions of the iron-core-less stator are shown on the 8 channels temperature output module, and the temperature data is collected through the PC for temperature real-time output with time interval of 10ms. A high precision torque-speed sensor is used to show the real rotating speed, and the speed-time curve is shown on the hose computer. The rotating speed for the temperature rise test experiment of the investigated motor of Type I in this paper are 6,000 rpm, 9,000 rpm, 12,000 rpm and 15,000 rpm.

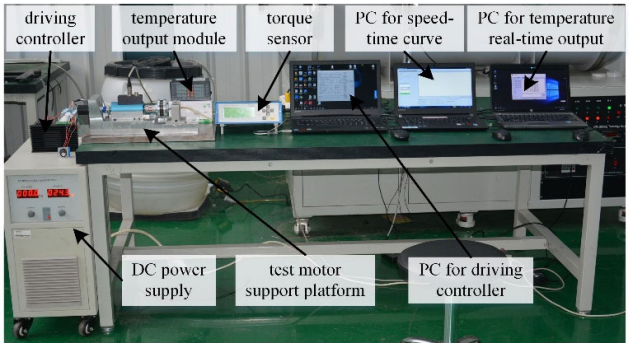

FIGURE 16. Temperature rise test system of the outer rotor and stator iron-core-less PMBLDC motor of Type I.

Fig.17∼Fig.19 show the temperature rise of different iron-core-less stator positions varying with different rotating speed of motors with three different combinations of number and diameter of parallel thin strand, i.e., 2 strands @ 0.75 mm, 4 strands @ 0.53 mm, and 11 strands @ 0.31 mm.

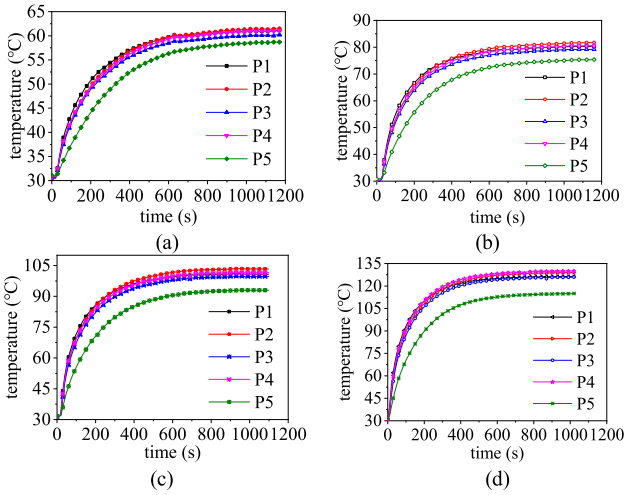

FIGURE 17. The temperature rise of different stator position varying with different rotating speed with combination of number and diameter of parallel thin strand of 2 strands @ 0.75 mm. (a) 6,000 rpm; (b) 9,000 rpm; (c) 12,000 rpm; (d) 15,000 rpm.

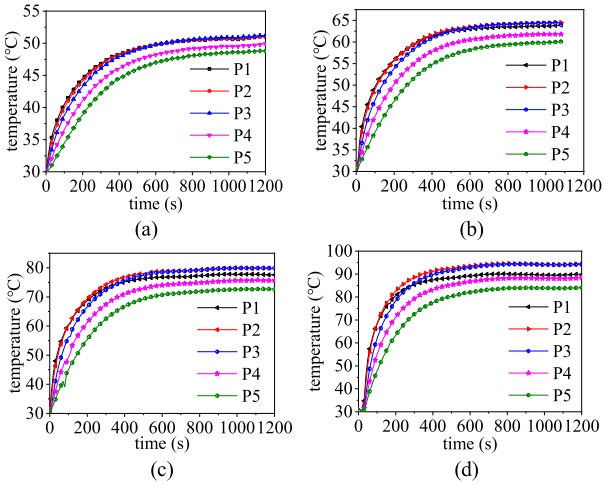

FIGURE 18. The temperature rise of different stator position varying with different rotating speed with combination of number and diameter of parallel thin strand of 4 strands @ 0.53 mm. (a) 6,000 rpm; (b) 9,000 rpm; (c) 12,000 rpm; (d) 15,000 rpm.

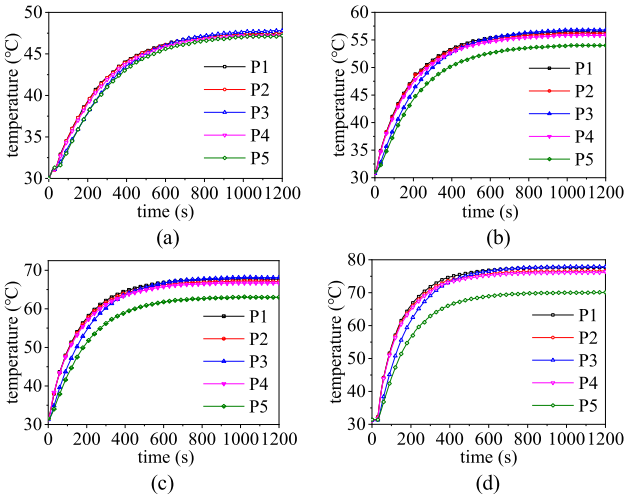

FIGURE 19. The temperature rise of different stator position varying with different rotating speed with combination of number and diameter of parallel thin strand of 11 strands @ 0.31 mm. (a) 6,000 rpm; (b) 9,000 rpm; (c) 12,000 rpm; (d) 15,000 rpm.

The steady state temperatures of the five measured positions of the Type I motor varying with the three combinations of number and diameter of parallel thin strand and the rotating speed are tabulated in Table 8. It can be seen that: 1) the steady state temperature of the winding getting higher and higher along with the strand diameter increasement at a certain rotating speed; 2) the temperature difference with a certain strand diameter getting bigger and bigger along with the rotating speed increasing; 3) for all the cases, the temperature differences of the four measured positions (P1∼P4) are not obvious, and the temperature of the center of the windings in the individual slot P2 is the highest; 4) the temperature difference between P5 and P2 getting bigger and bigger along with the rotating speed increasement with a certain strand diameter.

As is shown in Table 8, it should be noticed that, for the three combinations of number and diameter of parallel thin strands of Type I motor, the measured values of the steady state temperature rise at different stator positions varying with rotating speed of 2 stands @ 0.75 mm are basically consistent the simulation values of Fig.7. Due to the actual winding process limitation, the wire package cannot be guaranteed to be in an accurate spatial position. The error between the measured and simulated values within 4 strands @ 0.53 mm, and 11 strands @ 0.31 mm are large. Compared with the 2 stands @ 0.75 mm wire diameter combination, the number of parallel strands of other two wire diameter combinations increase.

The temperature rise experimental results of the three different combinations of strand diameter and parallel number in Fig.17 ∼ Fig.19 of certain stator position seems completely opposite with the simulation results in Fig.10. In [33] and [34], the results show both conductors transposition and wire twisting methods can make circulating current loss reduced more than 90%. As shown in Fig. 13, the winding twisting phenomenon indeed exists in manual winding process. Thus, the experimental measured circulating currents for the three cases can be ignored. The winding temperature rise of three combinations of strand diameter and parallel number only consider winding eddy current loss are obtained from the FEA. And the 3D FEA and experimental test results of winding temperature rise of Type I motor with the three combinations of strand diameter and parallel number versus rotating speed are shown in Fig.20. It can be found the experimental and simulated winding temperature rise for the cases of 2 strand @ 0.75 mm and 4 strands @ 0.53 mm show good agreement, respectively. Due to the wire twisting phenomenon of 11 strands @ 0.31 mm case is much serious than the other two cases, the temperature rise difference between the experiment and simulation results is a little higher.

TABLE 8. Steady-state temperature of the five measured positions with different strand diameter and rotating speed.

unit: W

Strand diameter	Measured position	Rotating speed (rpm) 6,000	9,000	12,000	15,000
0.75 mm	P1	61.2	80.3	100.8	126.3
	P2	61.5	81.7	103.3	128.8
	P3	60.2	79.2	99.6	126
	P4	61.1	80.5	101.5	130.1
	P5	58.8	75.5	93	115
0.53 mm	P1	51.3	63.9	77.8	89.9
	P2	51.4	64.5	80	94.5
	P3	51.6	64.5	80	94.5
	P4	50.3	61.8	75.2	88.3
	P5	49.3	60.1	72.7	84
0.31 mm	P1	47.5	56.5	67.6	77.7
	P2	47.4	56.2	67	76.6
	P3	47.8	56.8	68	78
	P4	47.2	55.8	66.5	76.1
	P5	47.1	54	65.8	70.1

It can be concluded by synthetically analysis that the contributions of the eddy and circulating current losses with different combinations of number and diameter of parallel thin strand to the thermal characteristics are different. The results show that the strand diameter has a great influence on the winding temperature rise, owing to the different eddy current losses with different strand diameters. If taking the circulating current losses into consideration, the temperature characteristics will be much different, which means the winding temperature with coarse strand diameter may smaller than that of thin strand diameter from the comprehensive study for minimizing losses of stator iron-core-less PMBLDC motors we have done. Hence, in order to reduce the temperature rise of the stator iron-core-less PMBLDC motors, the diameter and parallel number of the thin strand should be taken full consideration during the primary design process.

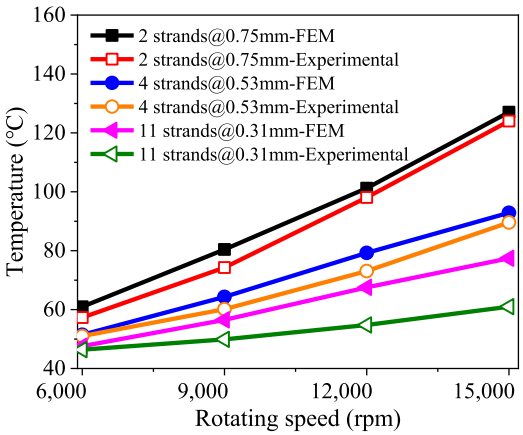

FIGURE 20. The 3-D FEA and experimental test results of winding temperature rise of Type I motor with three combinations of strand diameter and parallel number versus rotating speed.

V. CONCLUSION

In this paper, the influences on the thermal characteristic of three stator iron-core-less PMBLDC motors considering winding eddy and circulating current losses are investigated. Firstly, the effects of strand diameter, PMs' magnetization and rotating speed on the thermal characteristic of three stator iron-core-less PMBLDC motors are investigated by the 3D FEM. It is found that both strand diameter and rotating speed have big impacts on the temperature rise of three stator iron-core-less PMBLDC motors, and the parallel magnetization and radial magnetization have identical temperature rise results. Furthermore, the comprehensive effects of circulating and eddy current losses on the thermal characteristic of three stator iron-core-less PMBLDC motors are further studied. The results show that thermal analysis accounting the eddy and circulating current losses in parallel thin strands is very important during the primary design process because of the insulation level for winding and PM. Finally, three combinations of number and diameter of parallel thin strands, i.e. 2 strands @ 0.75 mm, 4 strands @ 0.53 mm, and 11 strands @ 0.31 mm, are selected for the temperature rising experiment. The experimental results and the FEM

results were compared and showed very good agreement. In this paper, three key influence factors on the temperature rise characteristics of this kind of coreless motor is clarified, which provides guidance for the design of this kind of motor. It indicates that the eddy current and circulating current presence in the parallel branches cannot be ignored in stator iron-core-less PMBLDC motors.

REFERENCES

[1] D. Mohanraj, R. Aruldavid, R. Verma, K. Sathiyasekar, A. B. Barnawi, B. Chokkalingam, and L. Mihet-Popa, "A review of BLDC motor: State of art, advanced control techniques, and applications," *IEEE Access*, vol. 10, pp. 54833–54869, 2022.

[2] M. S. Islam, R. Mikail, and I. Husain, "Slotless lightweight motor for aerial applications," *IEEE Trans. Ind. Appl.*, vol. 55, no. 6, pp. 5789–5799, Nov. 2019.

[3] C. Bianchini, A. Torreggiani, D. David, M. Davoli, and A. Bellini, "Fault tolerance analysis of an ironless PM machine for energy storage," *IEEE Energy Convers. Congr. Exposit. (ECCE)*, pp. 4499–4504, Oct. 2020.

[4] S. G. Min, "Analytical design and optimization of axial flux permanent magnet machines with slotless structure," *IEEE Trans. Transport Electrific.*, vol. 8, no. 2, pp. 1994–2004, Jun. 2022.

[5] S. Khan, S. S. H. Bukhari, and J.-S. Ro, "Design and analysis of a 4-kW two-stack coreless axial flux permanent magnet synchronous machine for low-speed applications," *IEEE Access*, vol. 7, pp. 173848–173854, 2019.

[6] J. Millinger, O. Wallmark, and J. Soulard, "High-frequency characterization of losses in fully assembled stators of slotless PM motors," *IEEE Trans. Ind. Appl.*, vol. 54, no. 3, pp. 2265–2275, May 2018.

[7] G. François and B. Dehez, "Impact of slit configuration on eddy current and supply current losses in PCB winding of slotless PM machines," *IEEE Trans. Ind. Appl.*, vol. 58, no. 5, pp. 6035–6044, Sep. 2022.

[8] B. Dong, K. Wang, B. Han, and S. Zheng, "Thermal analysis and experimental validation of a 30 kW 60000 R/min high-speed permanent magnet motor with magnetic bearings," *IEEE Access*, vol. 7, pp. 92184–92192, 2019.

[9] C. Luo, Y. Yang, and Z. Zhong, "Optimal braking torque distribution of dual-motor front-rear individually driven electric-hydraulic hybrid powertrain based on minimal energy loss," *IEEE Access*, vol. 10, pp. 134404–134416, 2022.

[10] K. Liu, M. Yin, W. Hua, Z. Ma, M. Lin, and Y. Kong, "Design and analysis of Halbach ironless flywheel BLDC motor/generators," *IEEE Trans. Magn.*, vol. 54, no. 11, pp. 1–5, Nov. 2018.

[11] K. Yamazaki, K. Utsunomiya, A. Tanaka, and T. Nakada, "Rotor surface optimization of interior permanent magnet synchronous motors to reduce both rotor core loss and torque ripples," in *Proc. IEEE Energy Convers. Congr. Exposit. (ECCE)*, Detroit, MI, USA, Oct. 2020, pp. 491–496.

[12] X. Huang, A. Goodman, C. Gerada, Y. Fang, and Q. Lu, "Design of a five-phase brushless DC motor for a safety critical aerospace application," *IEEE Trans. Ind. Electron.*, vol. 59, no. 9, pp. 3532–3541, Sep. 2012.

[13] J. Millinger, G. Bacco, V. Manzolini, O. Wallmark, and N. Bianchi, "Design and evaluation of a short-circuit rotor-ring for enhanced self-sensing capability in a slotless PM motor," *IEEE Trans. Ind. Electron.*, vol. 67, no. 5, pp. 3462–3471, May 2020.

[14] A. Boglietti, E. Carpaneto, M. Cossale, and S. Vaschetto, "Stator-winding thermal models for short-time thermal transients: Definition and validation," *IEEE Trans. Ind. Electron.*, vol. 63, no. 5, pp. 2713–2721, May 2016.

[15] S. Nategh, H. Zhang, O. Wallmark, A. Boglietti, T. Nassen, and M. Bazant, "Transient thermal modeling and analysis of railway traction motors," *IEEE Trans. Ind. Electron.*, vol. 66, no. 1, pp. 79–89, Jan. 2019.

[16] F. Zhang, D. Gerada, Z. Xu, X. Zhang, C. Tighe, H. Zhang, and C. Gerada, "Back-iron extension thermal benefits for electrical machines with concentrated windings," *IEEE Trans. Ind. Electron.*, vol. 67, no. 3, pp. 1728–1738, Mar. 2020.

[17] P. T. Luu, J.-Y. Lee, J.-H. Lee, and J.-W. Park, "Electromagnetic and thermal analysis of permanent-magnet synchronous motors for cooperative robot applications," *IEEE Trans. Magn.*, vol. 56, no. 3, pp. 1–4, Mar. 2020.

[18] R. Roy, S. Ramasami, and L. N. Chokkalingam, "Review on thermal behavior and cooling aspects of axial flux permanent magnet motors—A mechanical approach," *IEEE Access*, vol. 11, pp. 6822–6836, 2023.

[19] D. Lee, A. Yoon, S. Sirimanna, S. Salon, and K. S. Haran, "Impact of manufacturing tolerances on a low-reactance slotless PM synchronous machine," *IEEE Trans. Energy Convers.*, vol. 35, no. 1, pp. 366–374, Mar. 2020.

[20] X. Fan, B. Zhang, R. Qu, D. Li, J. Li, and Y. Huo, "Comparative thermal analysis of IPMSMs with integral-slot distributed-winding (ISDW) and fractional-slot concentrated-winding (FSCW) for electric vehicle application," *IEEE Trans. Ind. Appl.*, vol. 55, no. 4, pp. 3577–3588, Jul. 2019.

[21] B. Anvari, X. Li, H. A. Toliyat, and A. Palazzolo, "A coreless permanent-magnet machine for a magnetically levitated shaft-less flywheel," *IEEE Trans. Ind. Appl.*, vol. 54, no. 5, pp. 4288–4296, Sep. 2018.

[22] G. Du, W. Xu, J. Zhu, and N. Huang, "Power loss and thermal analysis for high-power high-speed permanent magnet machines," *IEEE Trans. Ind. Electron.*, vol. 67, no. 4, pp. 2722–2733, Apr. 2020.

[23] B. Han, X. Liu, Z. Huang, X. Zhang, and Y. Zhou, "Loss calculation, thermal analysis, and measurement of magnetically suspended PM machine," *IEEE Trans. Ind. Electron.*, vol. 65, no. 6, pp. 4514–4523, Jun. 2018.

[24] D. Liang, Z. Q. Zhu, J. Feng, S. Guo, Y. Li, A. Zhao, and J. Hou, "Simplified 3-D hybrid analytical modelling of magnet temperature distribution for surface-mounted PMSM with segmented magnets," *IEEE Trans. Ind. Appl.*, vol. 58, no. 4, pp. 4474–4487, Jul. 2022.

[25] J. G. Amorós, P. Andrada, B. Blanque, and M. Marin-Genesca, "Influence of design parameters in the optimization of linear switched reluctance motor under thermal constraints," *IEEE Trans. Ind. Electron.*, vol. 65, no. 2, pp. 1875–1883, Feb. 2018.

[26] C. T. Krasopoulos, A. S. Ioannidis, A. F. Kremmydas, I. A. Karafyllakis, and A. G. Kladas, "Convection heat transfer coefficient regression models construction for fast high-speed motor thermal analysis," *IEEE Trans. Magn.*, vol. 58, no. 11, pp. 1–5, Nov. 2022.

[27] S. Ahn, W. Song, and S. Min, "Multiobjective optimization of a traction motor in driving cycles using a coupled electromagnetic–thermal 1D simulation," *Int. J. Energy Res.*, vol. 2023, pp. 1–20, Nov. 2023.

[28] L. Yang, J. Zhao, W. Fu, X. Liu, J. Zhu, and C. Ai, "A comprehensive investigation of winding eddy and circulating current losses of stator iron coreless PMBLDC motors," *Energies*, vol. 16, no. 14, p. 5523, Jul. 2023.

[29] G. Wang, Z. Lyu, R. Gao, C. Tan, and X. Du, "An equivalent winding thermal model considering fill factor and void ratio for multiphysics coupling analysis of permanent magnet linear motors," *Appl. Thermal Eng.*, vol. 236, Jan. 2024, Art. no. 121605.

[30] H. Yin, F. Ma, X. Zhang, C. Gu, H. Gao, and Y. Wang, "Research on equivalent material properties and modal analysis method of stator system of permanent magnet motor with concentrated winding," *IEEE Access*, vol. 7, pp. 64592–64602, 2019.

[31] P. Liang, T. He, L. Liang, N. Jiao, and W. Liu, "Analytical thermal model of slot for electric propulsion motor in electric aircraft," *IEEE Trans. Energy Convers.*, vol. 38, no. 4, pp. 1–9, Jun. 2023.

[32] Y. Xia, S. Lv, B. Jing, and Z. Zhou, "Improvement of heat dissipation structure of low speed permanent-magnet motor," *IEEE Access*, vol. 11, pp. 51789–51797, 2023.

[33] D. Wang, Y. Liang, L. Gao, X. Bian, and C. Wang, "A new global transposition method of stator winding and its loss calculation in AC machines," *IEEE Trans. Energy Convers.*, vol. 35, no. 1, pp. 149–156, Mar. 2020.

[34] K. Yamazaki, T. Furuhashi, and S. Hara, "Separation of winding losses of permanent magnet motors by considering eddy currents and parallel circuit connections," *IEEE Trans. Magn.*, vol. 57, no. 6, pp. 1–4, Jun. 2021.

LIU YANG (Member, IEEE) was born in Hubei, China, in 1988. He received the B.E. degree in machine design manufacture and automation from Inner Mongolia University of Technology, Hohhot, China, in 2012, the M.Sc. degree in mechanical electronic engineering from Harbin Engineering University, Harbin, China, in 2015, and the Ph.D. degree in control science and engineering from Beijing Institute of Technology, Beijing, China, in 2020.

He is currently a Lecturer with the School of Mechanical Engineering, Yanshan University. His research interests include modeling and design of PM machines, high-precision servo control for positioning systems, fluid machinery and engineering, and mechatronic engineering.

TIANXIONG GAO was born in Xingtai, Hebei, China, in 1998. He received the B.S. degree in mechanical design and manufacturing and automation from Yanshan University, Qinhuangdao, in 2021, where he is currently pursuing the Ph.D. degree in fluid transmission and control.

His research interests include modeling and design of proportional electromagnet, PM machines, and high-precision servo control for positioning systems.

CHAO AI (Member, IEEE) was born in Tangshan, Hebei, China, in 1982. He received the B.S. degree in mechanical engineering and automation and the M.S. and Ph.D. degrees in fluid power transmission and control from Yanshan University, Qinhuangdao, China, in 2005, 2008, and 2013, respectively.

Since 2013, he has been with Yanshan University. From 2013 to 2015, he was a Lecturer with Yanshan University, where he is currently an Associate Professor, the Master's Supervisor, and the Ph.D. Supervisor. His current research interests include fluid power transmission and control, intelligent hydraulic wind power, fluid vibration and suppression, electro-hydraulic servo systems, and optimum design of hydraulic components.

XIANGDONG KONG was born in Qiqihar, Heilongjiang, China, in 1959. He received the B.S. degree in mechanical engineering from Zhejiang University, Hangzhou, China, in 1982, the M.S. degree in fluid power transmission and control from Northeast Heavy Machinery College, Qiqihar, in 1985, and the Ph.D. degree in fluid power transmission and control from Yanshan University, Qinhuangdao, China, in 1991.

Since 1991, he has been with Yanshan University. From 1991 to 1994, he was a Lecturer and an Associate Professor with Yanshan University. From 1994 to 1996, he was the Deputy Director of the Department of Mechanical and Electrical Control Engineering, Yanshan University, where he has been a Professor, since 1996. From 1996 to 1997, he was the Director of the President Office, Yanshan University. From 1997 to 2003, he was the Dean of the School of Mechanical Engineering, Yanshan University, where he has been the Vice President and the Ph.D. Supervisor, since 2003. His current research interests include fluid power transmission and control, intelligent hydraulic wind power, fluid vibration and suppression, electro-hydraulic servo systems, optimum design of hydraulic components, and theory and control of conveyor turbine.